DSTO

Removal of Range-dependent Artifacts from Sidescan Sonar Imagery

Stuart Anstee

DSTO-TN-0354

Removal of Range-dependent Artifacts from Sidescan Sonar Imagery

Stuart Anstee

Maritime Operations Division
Aeronautical and Maritime Research Laboratory

DSTO-TN-0354

ABSTRACT

A "radiosity correction" algorithm to improve the quality of sidescan sonar mosaics is reported. The algorithm removes consistent range-dependent variations from sidescan sonar imagery caused by failure of the TVG (time-varying gain) to completely compensate for variations due to transducer beam profiles and sediment backscatter strength. The correction is appropriate to high-frequency sidescan sonars with constant gain characteristics, such as the Klein 5000. The algorithm appears robust in situations where the bottom is relatively flat and the towfish altitude does not change much.

20010814 027

RELEASE LIMITATION

Approved for public release

DEPARTMENT OF DEFENCE
DEFENCE SCIENCE & TECHNOLOGY ORGANISATION **DSTO**

AQ FOI-11-2320

Removal of Range-dependent Artifacts from Sidescan Sonar Imagery

Executive Summary

Sidescan sonar mosaics are a geo-registered (map-like) form of seabed imagery with particular utility in mine hunting, route surveillance and hydrography. They can potentially provide high-quality information about sediment variations and object and obstacle locations. This report describes a simple "radiosity correction" algorithm to improve sidescan sonar mosaics that are subject to consistent range-dependent intensity variations.

The algorithm removes consistent range-dependent variations from sidescan sonar imagery caused by failure of the TVG (time-varying gain) to completely compensate for variations due to transducer beam profiles and sediment backscatter strength. The correction is appropriate to high-frequency sidescan sonars with constant gain characteristics, such as the Klein 5000.

The algorithm has proven effective for many high-resolution sidescan sonar collected with a Klein 5000 in Sydney Harbour and other areas. The algorithm appears to be very robust in situations where the bottom is relatively flat and the towfish altitude does not change much, a large proportion of most datasets. The algorithm imposes minimal processing overheads on modern personal computers.

The algorithm does not work effectively where the bottom is strongly sloping. It can also induce shading variations that are not directly associated with sediment type when the altitude of the towfish changes. The algorithm is not recommended for sediment classification; however, sediment boundaries are easier to see in mosaics prepared using the algorithm.

Contents

1. Introduction

Geo-registered or "mosaiced" sidescan sonar data provides a map-like view of the seabed with high potential value for applications such as mine countermeasures. However, the quality of a mosaic is very sensitive to defects in the data it incorporates. One of the defects commonly encountered is sometimes referred to as a "radiosity" effect. This is due to the vertical beam pattern of the transducers, which induce a consistent range-dependent variation in the signal level.

This report describes a simple "radiosity correction" algorithm that has proved effective in reducing range-dependent variations in imagery from the Klein 5000 sidescan sonar. The Klein 5000 operates at 455kHz. It is a short-range, high-resolution device with a relatively high signal to noise ratio across most of the swath, a factor that is important to the success of the algorithm. It also has fixed, operator-independent gain characteristics. This limits the number of different correction algorithms that must be developed.

The radiosity correction algorithm has been widely applied and appears to be quite robust. It is not greatly affected by the towing altitude of the towfish, the bottom type or the water depth. However, the algorithm has not been tested with data from lower-frequency sidescan sonars and its applicable frequency range has not been established.

Figure 1 Sidescan mosaic before (left) and after (right) correction for radiosity variations

Figure 1 shows an example of the effect of the radiosity correction. The bottom has areas of silt, shell-bed and rock. Sediment variations are suggested by differences in shading in the uncorrected image, but the cross-range shading variations make it difficult to identify boundaries between them. Sediment boundaries are much more readily visible in the corrected image. In particular, it is easy to see the exposed shell-bed that marks the vessel track going up to a wharf at the top-left of the image.

Mechanisms responsible for radiosity effects are discussed in Section 2 of this report, and some indication is given as to where the technique is likely to succeed.

The implementation and processing demands of the algorithm are discussed in Section 3, along with improvements that could be made in future.

2. Radiosity variations

2.1 Intensity variation with range

The total electrical response of the transducers can be described in terms of electrical power as:

$$P_T = \eta P_A + N_E \tag{2.1}$$

Here, P_T is the total electrical power induced in the system, η is the acoustic efficiency of the transducers and amplifiers, and N_E is the electrical noise power added by the system. After amplification, the total power is

$$P_S \cong g(t)P_A + 10^{NF/10} g(t)N_E \tag{2.2}$$

Here, $g(t)$ is the amplifier gain and NF is the noise factor of the amplifier system. Note that $g(t)$ is a "time-varying gain" with a value that is adjusted in an attempt to maintain the average output power approximately constant.

The acoustic power is the sum of "signal" power and "noise" power. For the purposes of bottom characterisation, the signal in this case is the part of the acoustic reverberation from the seabed that follows a direct path to and from the transducers. All other acoustic energy reaching the transducers is "noise", including surface and multipath reverberation and environmental noise. Hence,

$$P_A = P_A^S + P_A^N \tag{2.3}$$

The acoustic signal power is a function of the bottom characteristics, the geometry and the beam pattern via

$$P_A^S = P_0 \frac{\exp(-2\alpha r)}{r^4} b^2(\theta) s_b(\gamma) \qquad (2.3)$$

Here, the time-independent quantities are P_0, the power output of the transducer when it emits a pulse; α, the attenuation rate of sound in water; b, the transducer beam pattern; and s_b, the backscattering strength of the bottom. The others are time-dependent: $r=r(t)$, the one-way range (also known as the "slant range"); $\theta=\theta(t)$ is the start angle of the ray that will reach the bottom at range r, relative to the transducer surface normal – the "beam angle"; and $\gamma=\gamma(t)$ is the "grazing angle" that the ray makes where it contacts the bottom.

The acoustic noise power is a sum over contributions from the surface, ambient sources and multiple bottom/surface reflected energy ("multipaths"). Each of these terms has a form with similar complexity to (2.3).

Clearly, the power recorded by the system is a complicated function of the signal and multiple noise sources, which are in turn complicated functions of the topography, environmental characteristics and device characteristics. When the time-varying gain g of the system is imperfectly matched to the environment and the system, the radiosity effects seen in Figure 1 arise.

A correction to radiosity variations will only be feasible if most of the complicating effects are negligible. The regularity of the effect in Figure 1 suggests that this is so.

2.2 A simplified model

If we assume a flat sea bottom where the direct reverberation from the bottom (the signal) dominates other acoustic inputs to the transducers, and a low-noise sonar design, then the total electrical power recorded by the system will be approximated by

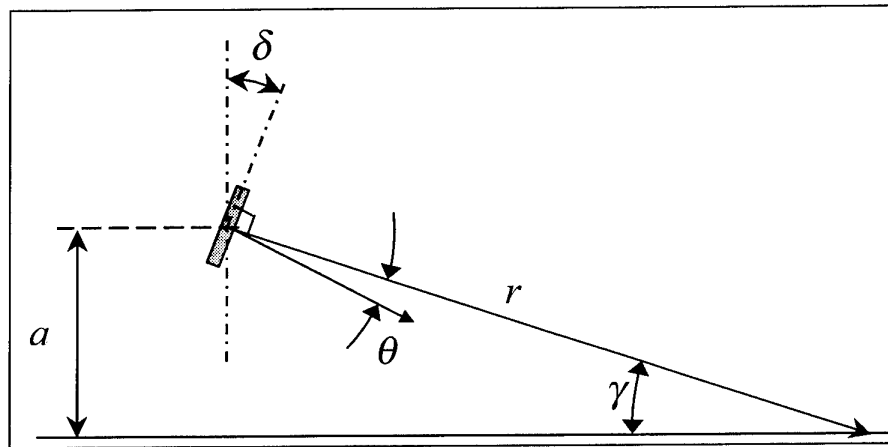$$P_A^S = \eta g(t) P_0 \frac{\exp(-2\alpha r)}{r^4} b^2(\theta) s_b(\gamma) \qquad (2.4)$$

If we further assume isovelocity propagation and a transducer tilt or depression angle of δ, then we have

$$\theta = \sin^{-1}\left(\frac{a}{r}\right) - \delta \qquad (2.5)$$

$$\gamma = \sin^{-1}\left(\frac{a}{r}\right) \qquad (2.6)$$

Here, the altitude of the transducers is a. The symbols referred to in equations (2.3) and following are depicted in Figure 2, which shows a transducer at altitude a, with its surface normal depressed by an angle δ. A point on the bottom at slant range r has an angle θ relative to the transducer face and sound waves strike the point with grazing angle γ.

Figure 2: Geometry of the sidescan swath, looking along-track

2.2.1 Geometrical dependencies

The rate of change of both angles is strongly range-dependent, since

$$\frac{d\theta}{dr} = \frac{d\gamma}{dr} = \frac{-1/r}{\sqrt{r^2/a^2 - 1}} \tag{2.7}$$

The rate of change is infinite at the nadir point where $a=r$, but falls rapidly as r becomes much larger than a. Given that sidescan sonars are deliberately towed close to the bottom, this is the case over much of the swath.

Figure 3 shows the variation of the beam angle with range for a few typical towing heights. Ranges out to 150m are displayed, but a Klein 5000 might typically be used with a 75m range setting. It would also normally be deployed less than 20m from the bottom.

Apart from the rapid change of beam angle near nadir, the curves in Figure 3 show that it is insensitive to range once the range has exceeded a few multiples of the towfish altitude. The form of the curves also becomes similar, and they approach each other in value. Finally, if the towfish is close to the bottom, the beam angle is also quite insensitive to the altitude.
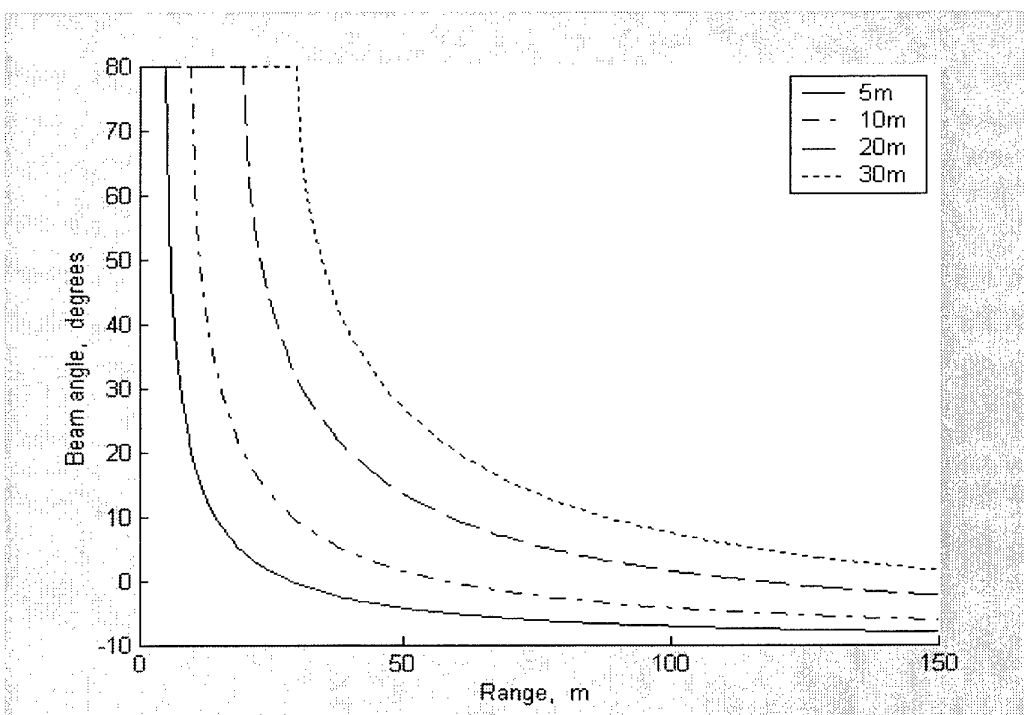
Figure 3 Variation of beam angle θ with slant range r from the sonar for some typical towfish altitudes. The transducer depression angle is 10° downward.

Equations (2.5) and (2.6) imply that the beam angle θ and grazing angle γ have the same variation with range. Grazing angle is thus insensitive to range and towfish altitude when the towfish is run close to the bottom. Hence, at long ranges from the sonar, a single radiosity correction may be valid for a range of altitudes if the beam pattern and backscatter strength vary only slowly with angle. This is unlikely to be the case closer to the sonar.

Figure 3 also implies that variations due to altitude will result in a constant shading offset at longer ranges, since the gradients of the curves are quite similar.

2.2.2 Backscatter variation

Backscatter models valid at 455kHz have not appeared in the literature to date. An empirical model published by the University of Texas [McKinney and Anderson 1964] is claimed to be valid for the frequencies from 20-290kHz. A semi-empirical model published by the Applied Physics Laboratory at the University of Washington [APL 1984, 1989, 1994] is claimed to be valid in the more restricted range 10-100kHz.
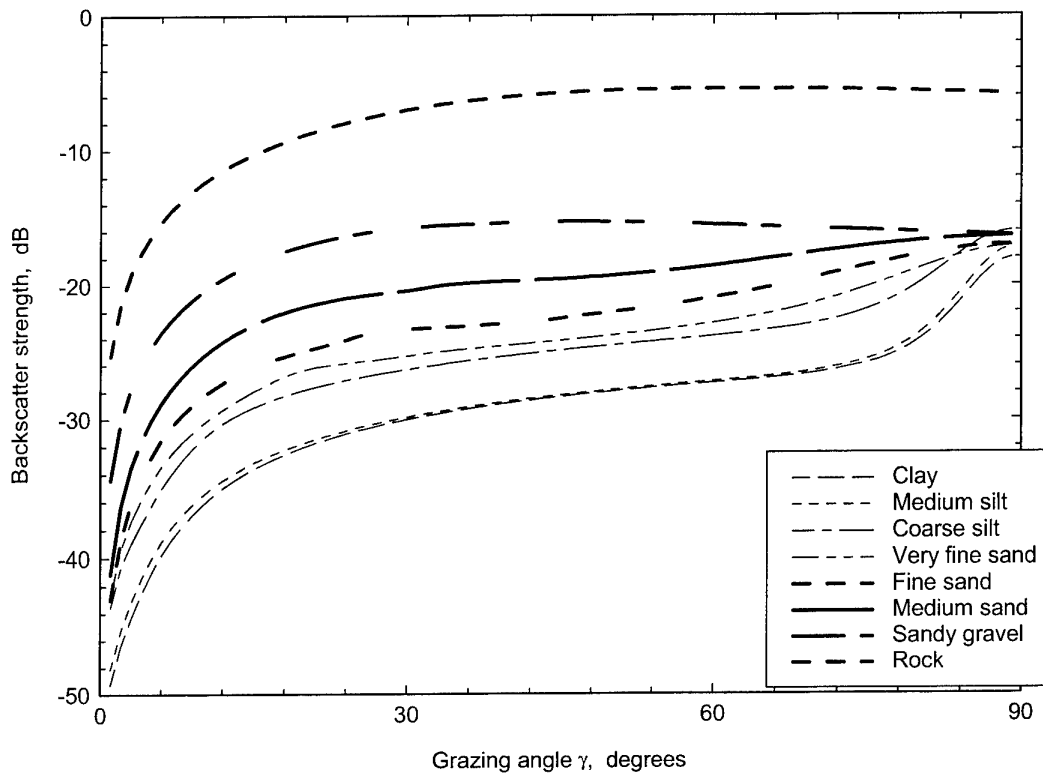
Figure 4 APL model predictions of bottom backscatter strength for generic sediment types at 455kHz.

In order to proceed, we must choose one of the models and use it well outside of its domain of validity. Given that the APL model is physically based, we assume that it will predict relative behaviour reasonably, even if the absolute values for the backscatter strength are incorrect.

Figure 4 shows bottom backscatter strength as a function of grazing angle for a range of "generic" sediment types. It is notable that at this high frequency, the curves do not cross, excepting at the highest grazing angles. All of the curves excepting sandy gravel have similar forms for grazing angles less than about 70°, implying that the backscattered intensity at a given angle should be a reasonably good indicator of sediment grain size.
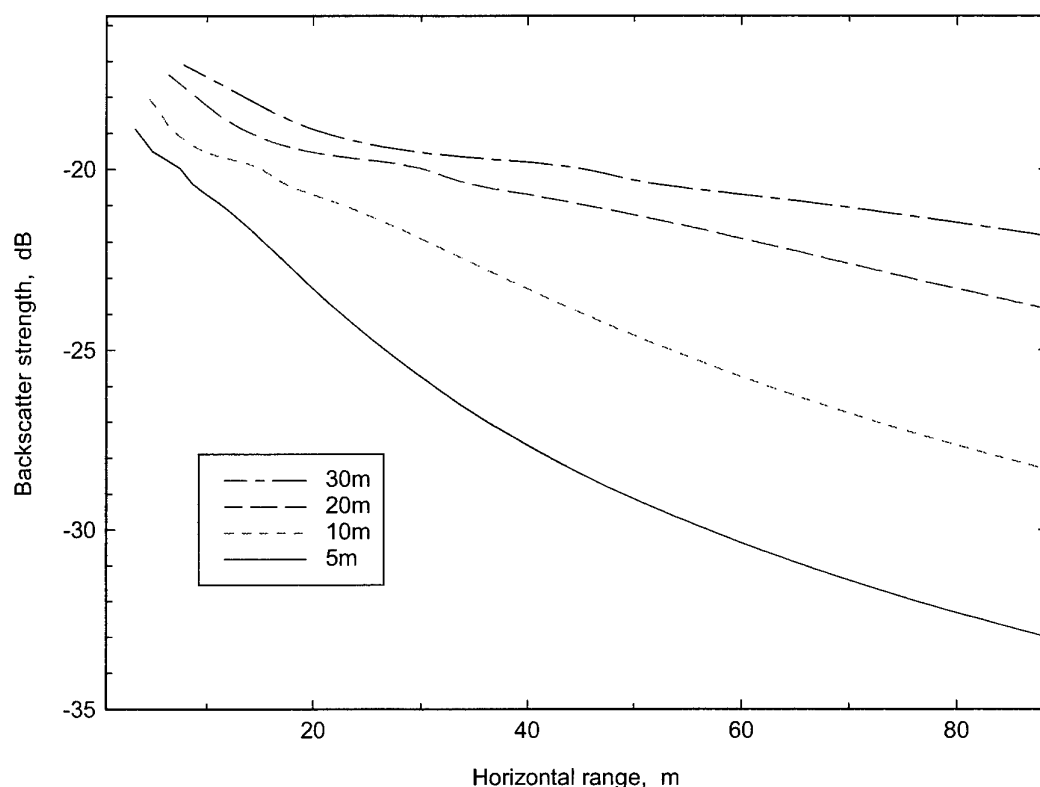
Figure 5 Bottom backscatter strength for 455kHz sound on a generic medium sand bottom as a function of range along the bottom and towfish altitude.

Figure 5 shows bottom backscatter strength as a function of horizontal range along the bottom for a generic "medium sand" bottom, at 455kHz. The predicted backscatter strength varies strongly as a function of both horizontal range and towfish altitude. The appearance of Figure 4 suggests that we can remove the variation with range almost independently of the sediment type. However, the variation with altitude would be more difficult to remove and would tend to make shallow areas appear acoustically less reflective. This means that a mosaic based on a range-dependent radiosity correction would not be useful for sediment classification unless the towfish were flown at a constant altitude from the bottom. A corrected mosaic may however still be useful for the location of sediment boundaries.

3. Radiosity correction algorithm

3.1 Processing order

The first decision that must be made when applying a radiosity correction is when to apply it, in particular, should the algorithm be applied before or after the sidescan data is projected from its original dependence on slant range (equivalently, time) to horizontal range across the bottom, so-called "slant-range corrected" data.

Figure 4 shows that the intensity variation in a sidescan sonar image is likely to be more rapid in the region of the nadir (high grazing angles) than elsewhere. The proportion of the image affected by this rapid variation is small (typically about 5%) when the data is projected as a function of the slant range and somewhat larger when it is projected as a function of horizontal range. For this reason, it was decided to apply the radiosity correction to the data before slant-range correction.

In the radiosity correction algorithm, all calculations start at the sample corresponding to the first bottom return – they are "bottom-tracking" and rely on an accurate determination of the location of the first bottom return. Samples corresponding to returns from the water column are ignored.

3.2 The filtration process

No single-stage filtration process investigated by the author appeared to be sufficient to remove range variations. Invariably, some variation remained in the near-nadir region. Hence, a two-stage process was adopted. First, variations away from the nadir region are removed with a fixed correction. Then, an adaptive correction is applied to remove the remaining variation near nadir.

3.2.1 First stage

Considering only one side of the sidescan data, let the time series of N_S samples for ping n be

$$s(n,i), \quad i = 0,1\dots N_S - 1 \tag{3.1}$$

Let the first bottom return for ping n be sample $i = b(n)$. We assume that a process exists for estimating $b(n)$ accurately.

Let N_{min} be the smallest number of 'on-land' samples per ping encountered during the averaging process, which is given by

$$N_{min} = \min(N_S - b(n)), \quad n = 1..N_P \tag{3.2}$$

Clearly, if a range-dependent variation is consistent from ping to ping, then it should become evident after averaging sufficiently many pings along track. However, the variation will follow the position of the first bottom return. Thus, we take a "bottom-tracking" average of the signal along the track, via

$$a(i) = \frac{1}{N_P} \sum_{n=0}^{N_P-1} s(n, i - b(n)), \, i = 0..N_{\min} \tag{3.3}$$

N_P is the total number of pings averaged along track. A value of $N_P = 200$ has been found to be adequate in this case.

Note that the average specified by N_P must be long enough to remove local variations, but not long enough to go from one major area of seabed sediment type to another.

After the first average, $a(i)$ remains a relatively unsmooth function. When applied directly, it causes streaks to appear along-track in the corrected image, corresponding to spikes in $a(i)$. To remove the spikes, a rolling average is applied across-track to smooth the function further, via

$$\bar{a}(i) = \frac{1}{q(i) - p(i) + 1} \sum_{j=p(i)}^{q(i)} a(j) \tag{3.4}$$

Here,

$$\begin{aligned} p(i) &= \max(0, i - l) \\ q(i) &= \min(N_{\min} - 1, i + l) \\ l &= N_{\min}/50 \end{aligned} \tag{3.5}$$

Finally, the average signal level for the entire area is evaluated. Let the across-track average of the along-track averages be A, given by

$$A = \frac{1}{N_{\min}} \sum_{i=0}^{N_{\min}-1} \bar{a}(i) \tag{3.6}$$

The first-stage correction is given by

$$C(i) = A/\max(1, \bar{a}(i)) \tag{3.7}$$

The correction is applied multiplicatively via

$$s_C(n, i) = C(i - b(n)) s(n, i) \tag{3.8}$$

Note again that the correction is tied to the first bottom return. Additive corrections do not work, since the beam pattern variation itself has a multiplicative effect on the signal level. Note also that the correction has no effect on the signal in the water column.

Figures 6 and 7 show the effects of the first stage correction on adjacent sections of data taken from one of the runs shown in Figure 1. Figure 6 shows the along-track averages of the port and starboard signal levels resulting from equation (3.3). Note that '0' slant range is the slant range at the first bottom return. There is clearly a large, systematic, range-dependent effect on both channels. The across-track smoothing effect of equation (3.4) on the port and starboard averages is shown by the cyan and green lines respectively.

Figure 7 shows the effect of applying the smoothed correction shown in Figure 6 to an adjacent section of data, via equations (3.7) and (3.8). Most of the systematic variation with range has been removed. Only a rapid variation in the first 3 metres remains.
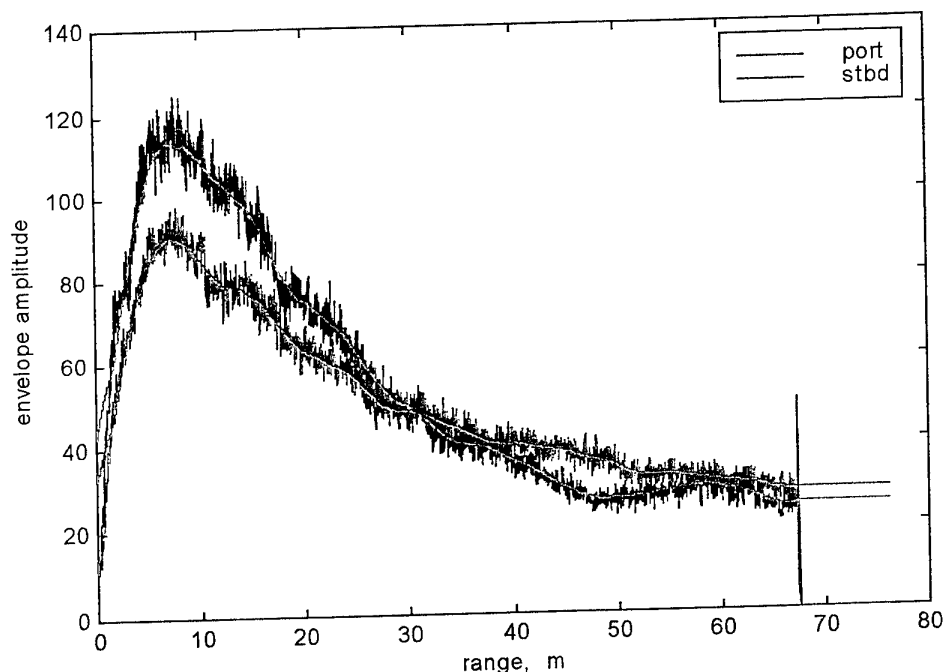

Figure 6 Sonar envelope voltages, averaged along-track, before correction
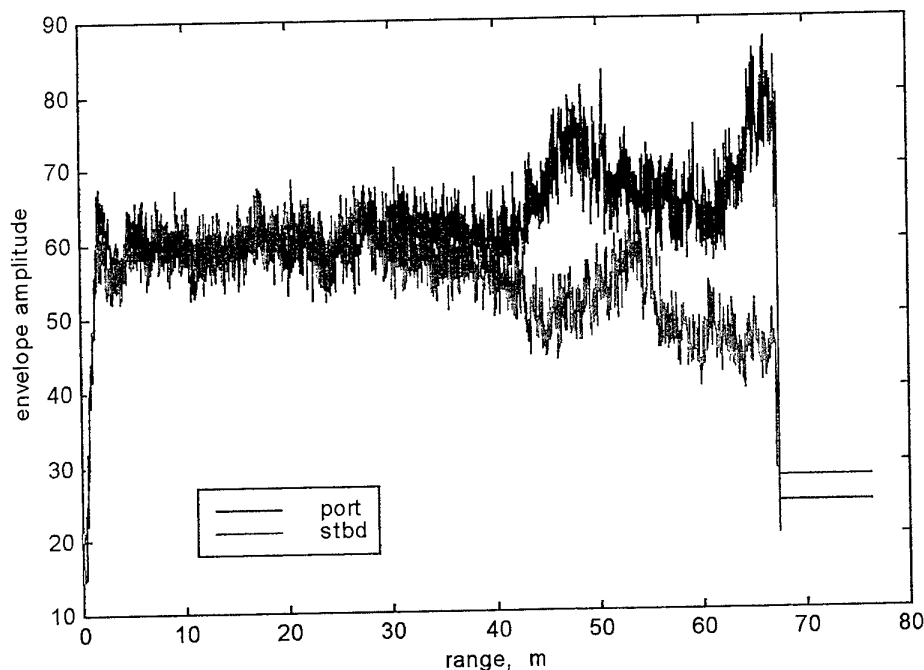
Figure 7 Sonar envelope voltages, averaged along-track, after first-stage correction

3.2.2 Second stage - near-nadir correction

After the initial correction has been applied, the image becomes more uniform, except in the near-nadir region where very rapid variations remain. A more local, adaptive correction is appropriate to this section of the image.

The near-nadir correction is based on the requirements that, at the point where the port and starboard images meet, they should have the same value and derivative. In this case, both 'value' and 'derivative' refer to time averages over scales appropriate to tonal variations. It is therefore assumed that, close to the nadir, the average variation of the signal level away from a straight line is a measure of the gain mismatch at that point.

In this case, the 'straight line' is taken to be the line between two 'anchor' points arbitrarily located 1/10th of the sonar range setting distant from the first bottom return. The value at each anchor point is estimated using a smoothing average along-track, via

$$v_n^\pm = \frac{1}{L}\left((L-1)v_{n-1} + s^\pm(n,b(n)+\Delta)\right) \tag{3.9}$$

Here, L is the length of the filter and Δ is the number of samples corresponding to $1/10^{th}$ of the range setting. The '+' and '−' symbols refer to port and starboard respectively, numbering samples outward from the towfish. An appropriate value of L has been experimentally determined to be 30, corresponding to movement of order 6m along-track.

In order to retain the detail in the near-nadir region, the same kind of along-track, smoothing average is applied to the data between the two anchor points. Let the value of each along-track average be $v_n(i)$, given by

$$v_n^{\pm}(i) = \frac{1}{L}\left((L-1)v_{n-1}(i) + s^{\pm}(n,b(n)+i)\right) \quad i = 0..\Delta-1 \tag{3.10}$$

The near-nadir correction is given by

$$c_n^{\pm}(i) = \left(\mu_n + (v_n^{\pm} - \mu_n)\frac{i}{\Delta}\right)\Bigg/ v_n^{\pm}(i) \quad i = 0..\Delta \tag{3.11}$$

$$\mu_n = (v_n^{+} + v_n^{-})/2$$

This is applied multiplicatively, via

$$\hat{s}_C^{\pm}(n,i) = c_n^{\pm}(i - b(n))\, s_C(n,i) \tag{3.12}$$

The final, corrected signal has been derived from the initially corrected signal by a multiplicative correction that does not act on the water column. Note that the value of the smoothing length L must be adjusted so that it is equivalent to several multiples of the largest expected details in the near-nadir region, but should otherwise be kept as small as possible.

Figure 8 shows along-track signal level averages for approximately the same section of data as Figure 7, after application of the second-stage correction given by equations (3.11) and (3.12). Longer ranges are unaffected by the correction, but the rapid change in the level in the first few metres of range has been removed. The port and starboard signal levels now approximately agree in both value and derivative.

The left and right halves of Figure 1 show a mosaic of the same data, before and after both stages of the correction algorithm have been applied. Clearly, the algorithm has been successful in this case in reducing the tonal variation at the centre of each line, and across the mosaic. The four lines in the mosaic may still be distinguished, but the underlying sediment variations (which have been confirmed by Roxann echo-sounder analysis and grab-sampling [Hamilton, 2000]) are clearly visible.
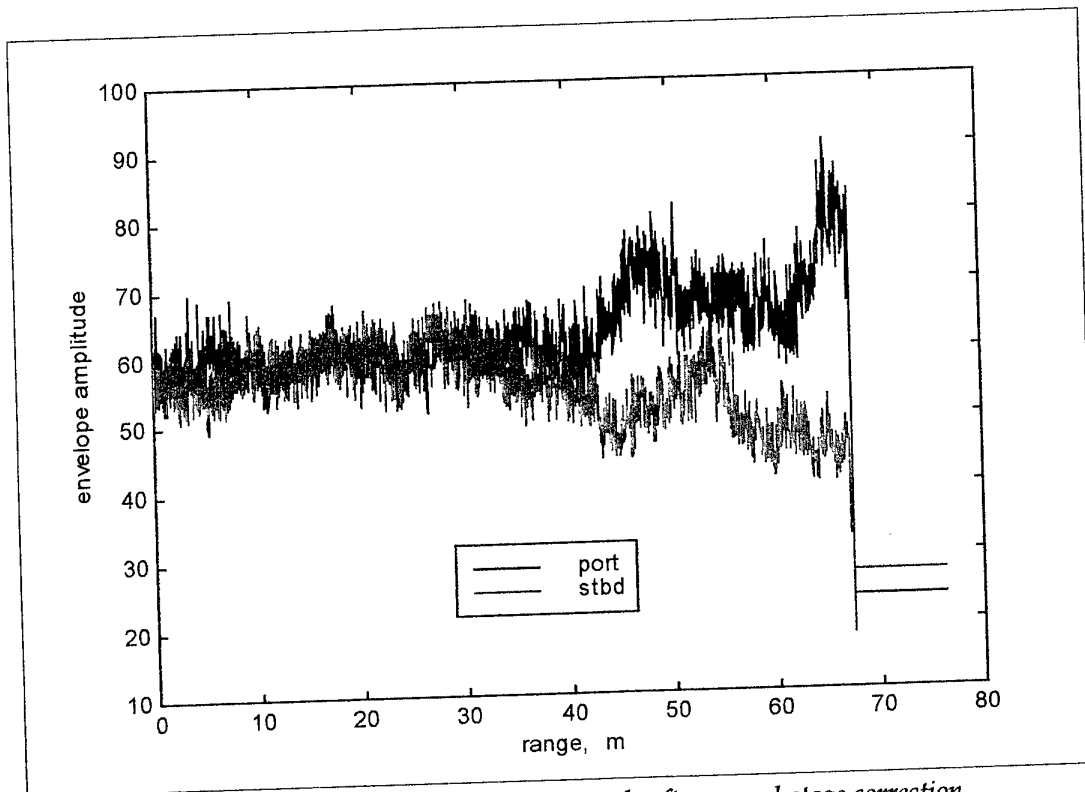
Figure 8 Sonar envelope voltages, averaged along-track, after second-stage correction

Figure 9 shows the two stages of the correction acting on a segment of sidescan sonar raster imagery. The data is not corrected for slant range. The movement of the sonar is from right to left on the page. The dark horizontal band at centre of each image is a clipped region due to the emission of each ping, and the clear areas above and below it are the returns from the water column.

The uncorrected image on the left of Figure 9 has light bands immediately following the first returns from the bottom, relatively dark areas at mid-range and increasingly lighter tones at larger ranges. Both light and dark bands are clearly visible in the uncorrected mosaic in Figure 1. The tone corresponds to the signal level, which is highest at intermediate ranges. The reason that a filtering process is important in the production of mosaiced images is evident from Figure 1. The regions of sharp variation from below-average to above-average signal level immediately adjacent the first bottom return take up a larger portion of the image when they are projected onto a horizontal plane representing "true range".

After stage 1 of the radiosity correction, the image appears like the centre part of Figure 9, which now has narrow dark bands (over-correction) immediately following the first bottom returns, but does not have the tonal fall-off at long ranges, or the peak at mid-ranges.

13

After stage 2 of the correction, the final image appears like the right third of Figure 9, which has even tonal variation at all ranges.
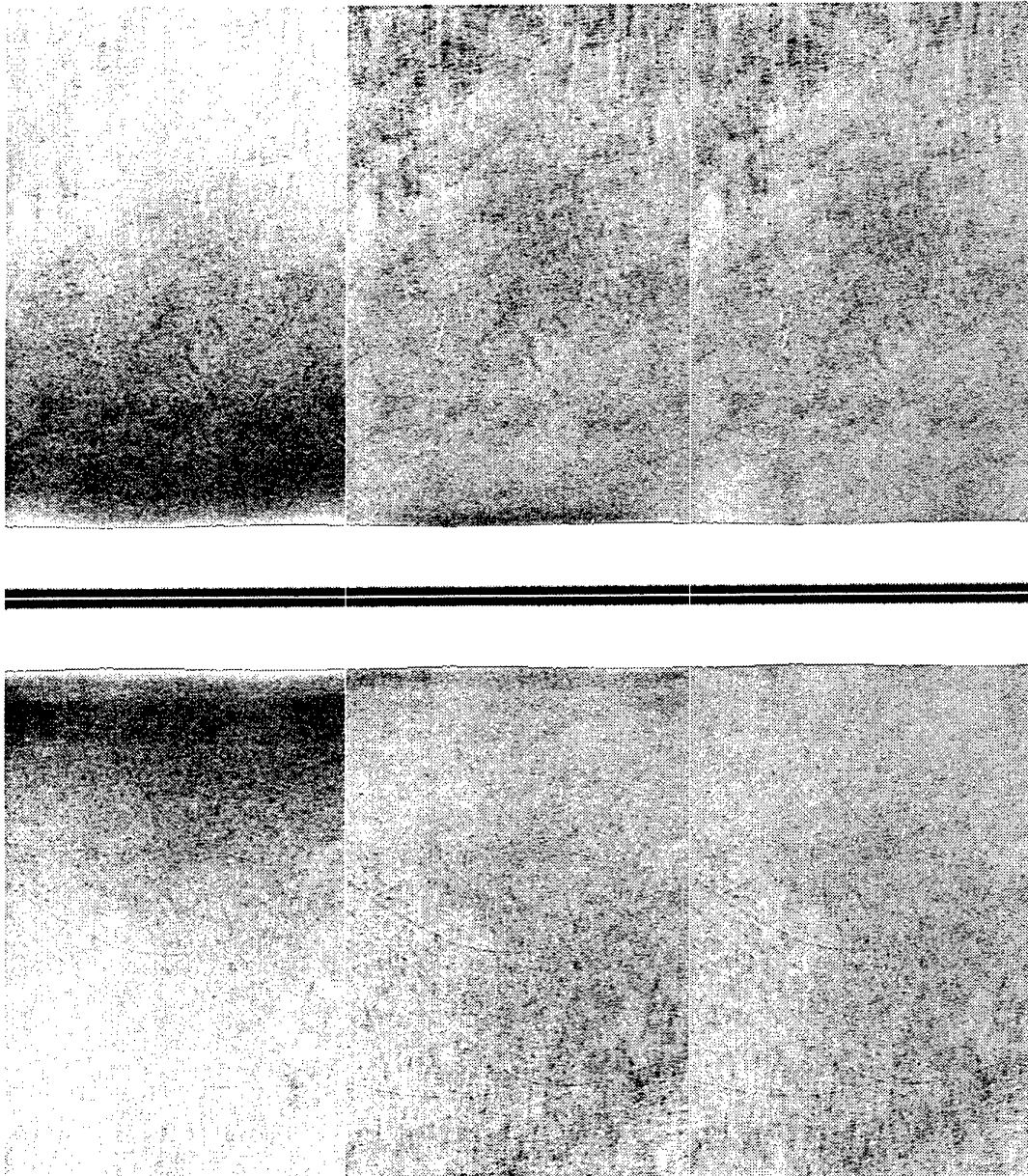

Figure 9 Sidescan sonar raster data, uncorrected (left), after stage 1 (centre) and after stage 2 (right).

4. Limitations

The radiosity correction in this report has been tested with sets of data from various versions of the Klein 5500 sidescan sonar. It has been successful where data was collected over a relatively flat seabed.

The primary limitation of the correction is that it cannot normalise tonal variations over sloping ground, particularly when runs are not parallel to each other. The backscatter coefficient in equation (2.4) is dependent on the grazing angle that the sediment patch makes relative to the sonar, and this will generally be different when the sonar views a sloping area from two different aspects.

A second limitation is the depedence of the shading on towfish altitude. The radiosity correction does not attempt to correct for the reduction in signal level when the towfish is flown closer to the bottom. Hence, mosaics made with this technique cannot be used for sediment classification unless the towfish altitude has been held constant.

A third limitation is due to the pointwise nature of the algorithm, which was adopted to minimise processing time. Were a faster processor available, it would be better to express the correction as a polynomial function of either range or grazing angle. This would avoid problems in very shallow water, where the number N_{min} of samples defined in equation (3.3) can be somewhat larger than it is when the towfish is flown higher. In effect, a shallow-water correction can be used for deeper water, but not vice-versa.

Figure 10 shows a mosaic incorporating the flat area shown in Figure 1 at the left side of the image, but also incorporating stongly sloping regions. The mosaic is aligned with north up in the usual way. The areas to the east, west and southeast of the central peninsula are quite flat, but a deep hole is located in the south and southwest. In this sloping region, clear tonal variations can be seen between runs, sufficient to obscure features of interest. Elsewhere, tonal variations are due to sediment changes from shell-beds (dark) to mud (light).

Note that some of the tonal variation in the shallow water to the northeast may be due to a reduction in towfish altitude, but the sediment is silty and hence has a low backscatter strength.

The technique has not been trialled with 100kHz data, which may exhibit a less uniform variation of backscatter coefficient with sediment type than is observed at 455kHz. If backscatter strength curves for different sediments cross at low or medium grazing angles, then the correction will fail on flat ground.

Figure 10 Sidescan mosaic showing breakdown of TVG compensation in a sloping region

5. Conclusion

This report has demonstrated a simple technique for removal of range-dependent artifacts from mosaics prepared using Klein 5000 sidescan sonar data. It should work equivalently for other digital sonars with similar characteristics. The correction improves the quality of the mosaics so that they are more useful for sediment classification purposes.

The crucial factors are separate treatment of the data in the nadir region; a non-adaptive correction for the non-nadir region; and application of the radiosity correction before slant-range correction.

The correction is probably limited to frequencies at the higher end of the range, say above 200kHz. It is also limited to data collected over approximately level ground and with a constant towfish altitude.

16

6. References

APL (1984, 1989, 1994) *APL-UW High-frequency ocean environmental acoustic models handbook*, Applied Physics Laboratory Technical Report APL-UW TR 8407, APL-UW TR 8907 and APL-UW TR 9407. Most recent issue supersedes previous issues. Applied Physics Laboratory, University of Washington, 1013 NE 40th Street, Seattle, Washington, 98105-6698.

Hamilton, L. J. (2000) Private communication. Mr Hamilton is a Professional Officer in the Maritime Operations Division, DSTO, PO Box 44, Pyrmont, NSW 2009, Australia.

McKinney, C. M. and Anderson, C. D. (1964) Measurements of backscattering of sound from the ocean bottom, *J. Acoust. Soc. Am.* **36**, 158-163.

DISTRIBUTION LIST

Removal of Range-Dependent Artifacts from Sidescan Sonar Imagery

S.D. Anstee

AUSTRALIA

DEFENCE ORGANISATION

Task Sponsor
COMAUSNAVMCDGRP

S&T Program
Chief Defence Scientist ⎫
FAS Science Policy ⎬ shared copy
AS Science Corporate Management ⎪
Director General Science Policy Development ⎭
Counsellor Defence Science, London (Doc Data Sheet)
Counsellor Defence Science, Washington (Doc Data Sheet)
Scientific Adviser to MRDC Thailand (Doc Data Sheet)
Scientific Adviser Policy and Command
Navy Scientific Adviser
Scientific Adviser - Army (Doc Data Sheet and distribution list only)
Air Force Scientific Adviser
Director Trials

Aeronautical and Maritime Research Laboratory
Director
Chief of Maritime Operations Division
Research Leader Mine Warfare
Brian Ferguson, MOD Sydney
Stuart Anstee, MOD Sydney
Philip Chapple, MOD Sydney
Philip Mulhearn, MOD Sydney
Amy Young, MOD Sydney
Roger Neill, MPD, MB

DSTO Library and Archives
Library Fishermans Bend (Doc Data Sheet)
Library Maribyrnong (Doc Data Sheet)
Library Salisbury
Australian Archives
Library, MOD, Pyrmont (2 Copies)
Library, MOD, HMAS Stirling
*US Defense Technical Information Center, 2 copies
*UK Defence Research Information Centre, 2 copies
*Canada Defence Scientific Information Service, 1 copy
*NZ Defence Information Centre, 1 copy
National Library of Australia, 1 copy

Capability Systems Staff
Director General Maritime Development
Director General Aerospace Development (Doc Data Sheet only)

Knowledge Staff
Director General Command, Control, Communications and Computers (DGC4)
(Doc Data Sheet only)
Director General Intelligence, Surveillance, Reconnaissance, and Electronic
Warfare (DGISREW)R1-3-A142 CANBERRA ACT 2600 (Doc Data Sheet
only)
Director General Defence Knowledge Improvement Team (DGDKNIT)
R1-5-A165, CANBERRA ACT 2600 (Doc Data Sheet only)

Navy
SO (Science), Director of Naval Warfare, Maritime Headquarters Annex,
Garden Island, NSW 2000. (Doc Data Sheet only)
DDMWD (CMDR Roger Dobson)
MHD (LCDR Peter Johnson)

Army
Stuart Schnaars, ABCA Standardisation Officer, Tobruck Barracks, Puckapunyal,
3662 (4 copies)

Intelligence Program
DGSTA Defence Intelligence Organisation
Manager, Information Centre, Defence Intelligence Organisation

Corporate Support Program
OIC TRS, Defence Regional Library, Canberra

UNIVERSITIES AND COLLEGES
Australian Defence Force Academy Library
Senior Librarian, Hargrave Library, Monash University
Librarian, Flinders University

OTHER ORGANISATIONS

NASA (Canberra)
AGPS
Klein Associates Inc., 11 Klein Drive, Salem, New Hampshire 03079, USA
Triton Elics International, 125 Westridge Drive, Watsonville CA 95076, USA

OUTSIDE AUSTRALIA

ABSTRACTING AND INFORMATION ORGANISATIONS
Library, Chemical Abstracts Reference Service
Engineering Societies Library, US
Materials Information, Cambridge Scientific Abstracts, US
Documents Librarian, The Center for Research Libraries, US

INFORMATION EXCHANGE AGREEMENT PARTNERS
   Acquisitions Unit, Science Reference and Information Service, UK
   Library - Exchange Desk, National Institute of Standards and Technology, US

SPARES (5 copies)

Total number of copies: 55

DEFENCE SCIENCE AND TECHNOLOGY ORGANISATION DOCUMENT CONTROL DATA		1. PRIVACY MARKING/CAVEAT (OF DOCUMENT)

2. TITLE Removal of Range-dependent Artifacts from Sidescan Sonar Imagery	3. SECURITY CLASSIFICATION (FOR UNCLASSIFIED REPORTS THAT ARE LIMITED RELEASE USE (L) NEXT TO DOCUMENT CLASSIFICATION) Document (U) Title (U) Abstract (U)

4. AUTHOR(S) Stuart Anstee	5. CORPORATE AUTHOR Aeronautical and Maritime Research Laboratory 506 Lorimer St Fishermans Bend Vic 3207 Australia

6a. DSTO NUMBER DSTO-TN-0354	6b. AR NUMBER AR-011-850		6c. TYPE OF REPORT Technical Note	7. DOCUMENT DATE April 2001
8. FILE NUMBER 490-6-47	9. TASK NUMBER NAV 00/037	10. TASK SPONSOR COMAUSNAVMCDGRP	11. NO. OF PAGES 17	12. NO. OF REFERENCES 3

13. URL ON WORLDWIDE WEB http://www.dsto.defence.gov.au/corporate/reports/DSTO-TN-0354.pdf	14. RELEASE AUTHORITY Chief, Maritime Operations Division

15. SECONDARY RELEASE STATEMENT OF THIS DOCUMENT

Approved for public release

OVERSEAS ENQUIRIES OUTSIDE STATED LIMITATIONS SHOULD BE REFERRED THROUGH DOCUMENT EXCHANGE, PO BOX 1500, SALISBURY, SA 5108

16. DELIBERATE ANNOUNCEMENT

No Limitations

17. CASUAL ANNOUNCEMENT	Yes

18. DEFTEST DESCRIPTORS

Acoustic Imaging; Route Surveys; Towed Sonar; Sediment classification

19. ABSTRACT
A "radiosity correction" algorithm to improve the quality of sidescan sonar mosaics is reported. The algorithm removes consistent range-dependent variations from sidescan sonar imagery caused by failure of the TVG (time-varying gain) to completely compensate for variations due to transducer beam profiles and sediment backscatter strength. The correction is appropriate to high-frequency sidescan sonars with constant gain characteristics, such as the Klein 5000. The algorithm appears robust in situations where the bottom is relatively flat and the towfish altitude does not change much.

DEPARTMENT OF DEFENCE

DEFENCE SCIENCE & TECHNOLOGY ORGANISATION

DSTO